RSC Advances

This is an *Accepted Manuscript*, which has been through the Royal Society of Chemistry peer review process and has been accepted for publication.

Accepted Manuscripts are published online shortly after acceptance, before technical editing, formatting and proof reading. Using this free service, authors can make their results available to the community, in citable form, before we publish the edited article. This *Accepted Manuscript* will be replaced by the edited, formatted and paginated article as soon as this is available.

You can find more information about *Accepted Manuscripts* in the Information for Authors.

Please note that technical editing may introduce minor changes to the text and/or graphics, which may alter content. The journal's standard Terms & Conditions and the Ethical guidelines still apply. In no event shall the Royal Society of Chemistry be held responsible for any errors or omissions in this *Accepted Manuscript* or any consequences arising from the use of any information it contains.

ROYAL SOCIETY OF CHEMISTRY

www.rsc.org/advances

Please do not adjust margins

Journal Name

ARTICLE

Ionic liquid-assisted growth of methylammonium lead iodide spherical nanoparticles by a simple spin-coating method and photovoltaic properties of perovskite solar cells

Received 00th January 20xx,
Accepted 00th January 20xx

DOI: 10.1039/x0xx00000x

www.rsc.org/

Md. Shahiduzzaman,[a*] Kohei Yamamoto,[a] Yoshikazu Furumoto,[a] Takayuki Kuwabara,[a,b] Kohshin Takahashi,[a,b] and Tetsuya Taima[a,b*]

Hybrid organometal halide perovskites such as methylammonium lead iodide ($MAPbI_3$) are a promising class of cost- and energy-efficient light absorption materials for thin-film photovoltaics. In this work, the preparation and characterization of $MAPbI_3$ nanoparticles (NPs) on TiO_x/indium tin oxide glass substrates using a simple spin-coating technique have been investigated. The NPs were prepared by spin-coating solutions of $MAPbI_3$ and the ionic liquid (IL) 1-hexyl-3-methylimidazolium chloride in N,N-dimethylformamide. Analysis of the resulting spin-coated films revealed that uniform spherical $MAPbI_3$ NPs with an average diameter of 540 nm were homogeneously distributed on the TiO_x substrates. $MAPbI_3$ films with similar crystallinity were observed irrespective of the inclusion of IL, as evident from the X-ray diffraction patterns of the films. However, addition of IL to the spin-coating solution facilitated the formation of homogenous nucleation sites and prevented rapid crystal formation of $MAPbI_3$. Therefore, the presence of an IL resulted in uniform thin films with good morphology.

Introduction

Perovskites show potential for application in multiple fields such as superconductors,[1] sensors,[2] fuel cells,[3] ferroelectric,[4, 5] photocatalysis,[6] batteries,[7, 8] and thermoelectrics.[9] Semiconductor nanostructures have opened the door for the use of nanocrystalline pigments as attractive light harvesters, which have the following characteristics: a) The nanostructure of the light absorber layer possesses sub-wavelength features because of quantum size effects, which results in very low reflection and increased photon absorption and provides higher cell efficiency without the need for additional antireflection coatings; b) The large surface areas of nanotextured materials allow efficient energy conversion and charge–carrier recombination.[10] Among semiconducting materials, low-dimensional layered compounds have been intensely investigated as a promising candidate for organic–inorganic-based perovskites.[11] Complex-shaped perovskite nanoparticles (NPs) can be one-dimensional (nanowires, nanotubes, and nanorods), two-dimensional (nanodiscs, nanoplatelets, and nanosheets), or other complex shapes such as rod-sheet heterogeneous NPs. To date, there have been many reports on quantum wells,[12, 13] wires,[14] and dots[15] synthesized from organic–inorganic perovskite compounds. While numerous synthetic approaches have been used to prepare nanoscale perovskite materials, those based on chemical synthesis offer the most versatility in terms of the manipulation of the characteristics of individual particles, including size, shape, and structure or surface properties. Chemical synthetic techniques are advantageous for large-scale tailored production of anisotropic perovskite NPs, which can be readily assembled into nanostructured bulk perovskite materials with highly efficient properties for practical applications. Several chemical synthetic methods have been developed to prepare complex-shaped metal perovskite NPs, including the hydrothermal/ solvothermal method[16-18] and wet chemical synthesis.[19] However, researchers are interested in developing thin-film perovskite materials by simple, cost-effective, and precise techniques as an alternative to chemical synthesis. Spin coating is a common, cheap, simple, and precise film production method, in which a centrifugal force is used to produce uniform solution-processed thin films. Centrifugal force causes a dispersion to spread uniformly across a substrate, which is followed by evaporation of the solvent to yield a thin particle film.[20]

Schmidt et al.,[21] reported the synthesis of methylammonium lead bromide NPs by a simple spin-coating method on a quartz substrate with the objective of fabricating nanostructured

[a] Graduate School of Natural Science and Technology, Kanazawa University, Kakuma, Kanazawa 920-1192, Japan
[b] Research Center for Sustainable Energy and Technology, Kanazawa University, Kakuma, Kanazawa 920-1192, Japan
*E-mail: shahiduzzaman09@gmail.com (MS); taima@se.kanazawa-u.ac.jp (TT)
Tel./Fax: +81-76-264-6279

Electronic Supplementary Information (ESI) available: Information of the Peak parameters used to calculate the mean crystalline size in films formed with and without IL by the Scherrer formula].
See DOI: 10.1039/x0xx00000x

RSC Advances Accepted Manuscript

Please do not adjust margins

organic lead halide perovskite for use in the solar cells. Moreover, $MAPbI_3$ nanowires have been prepared by a low-temperature solution process using a simple slip-coating method[22] for solar cells. Control of morphology and crystallization are the main challenges encountered in perovskite-based thin films and affect the quality of the resulting film. The morphology of non-homogeneous thin films can limit device performance because of electrical shorting, or effects on charge dissociation/transport/recombination.[23-25] Therefore, an easy scalable efficient approach to fabricate homogeneous perovskite films with controlled morphology for use in perovskite solar cells needs to be developed.

In the present study, we use a simple spin-coating technique to fabricate uniformly distributed spherical NPs of $MAPbI_3$ in the presence of the ionic liquid (IL) 1-hexyl-3-methylimidazolium chloride (HMImCl), which is introduced to control morphology. HMImCl has a high boiling point, extremely low vapor pressure, high ionic conductivity, and excellent electrochemical and high thermal stability.

Experimental

Chemicals

Lead iodide (PbI_2, purity 98%) was purchased from Tokyo Chemical Industry (Tokyo, Japan), while titanium (IV) oxysulfate ($TiOSO_4$, purity 99.99) and 1-hexyl-3-methylimidazolium chloride (HMImCl, purity 97%) were from Sigma Aldrich (St. Louis, MO, USA). Hydrogen peroxide (H_2O_2, purity 35%) and N,N-dimethylformamide (DMF, purity 99.5%) were supplied by Kanto Chemical (Tokyo, Japan).

Instrumentation

The scanning electron microscopy (SEM) and Energy-dispersive X-ray spectroscopy (EDX) (SU1510, Hitachi High-Tech, Tokyo, Japan) were used to analyse to analyse the surface morphology and elemental mapping. Surface morphology was further investigated by atomic force microscopy (AFM; SII SPI3800N, Seiko, Japan). Ultraviolet-visible (UV-Vis) absorption spectra of perovskite films were measured using an absorption spectrophotometer (U-3310, Hitachi, Tokyo, Japan). X-ray diffraction (XRD) patterns of the prepared films were measured using an X-ray diffractometer (SmartLab, Rigaku, Japan) with an X-ray tube (Cu Kα, λ = 1.5406 Å). A further analysis of the films was performed using Fourier Transform Infrared Spectroscopy (FTIR) with Infrared Reflection Absorption Spectroscopy (IRRAS) (FT/IR-6300, Jasco, Tokyo, Japan).

Methods

Substrate cleaning

Indium tin oxide (ITO)-patterned glass substrates purchased from Techno Print Co., Ltd. (Saitama, Japan) were treated with oxygen plasma for 20 min prior to use.

Preparation of compact-TiO_x films by chemical bath deposition (CBD)

Compact-TiO_x layers were prepared in aqueous solutions of $TiOSO_4$ (1.6 g) and H_2O_2 (0.17 g) at 80 °C via CBD.[26, 27] The chemical bath was purchased from AS-One (EO-200, Tokyo, Japan). The deposited compact-TiO_x films were heated on a hot plate (ND1, AS-One, Tokyo, Japan) at 150 °C for 1 h to obtain amorphous films.

Preparation of $MAPbI_3$ NCs by spin coating

Lead iodide (PbI_2) (0.144 g) and methylammonium iodide (MAI) (0.05 g) were mixed in anhydrous DMF (615 µL) at 2.89:1 molar ratio by shaking (VMR-5R, AS-One) at room temperature (RT) for 30 min to produce a clear $MAPbI_3$ solution with a concentration of 25 wt%. PbI_2 was dehydrated under vacuum at 450 °C for 3 h prior to use. Methylamonium lead iodide (MAI) was synthesized in our laboratory. A compact-TiO_x layer (30 nm) was deposited on ITO-coated glass substrates using CBD technique as described earlier. The DMF solution of $MAPbI_3$ (25 wt%) were spin coated on top of the amorphous compact- TiO_x layer at 3000 rpm. During spin coating, the color of the film changed from transparent to peach. The film was left to dry at RT for 30 min to allow slow solvent evaporation, followed by annealing on a hot plate at 100 °C for 10 min, giving a $MAPbI_3$ film with a thickness of 200 nm. The whole process was performed in an N_2-filled glove box.

Preparation of $MAPbI_3$ NPs by spin coating

$MAPbI_3$ NPs were prepared using the same spin-coating technique as that described in preparation of $MAPbI_3$ NCs, except that 1 wt% HMImCl was also included in the 25 wt% $MAPbI_3$ solution in DMF.

Solar Cell Fabrication using $MAPbI_3$ NPs

The hole-transporting layer (HTM) was produced using 2,2′,7,7′-tetrakis (N,N-di-p-methoxyphenylamine)-9,9′-spirobifluorene (spiro-OMeTAD) via spin-coating at 4000 rpm over the $MAPbI_3$ NPs layer. The spiro-OMeTAD in chlorobenzene (0.058 M) was prepared using 4-tert-butylpridine (0.19 M), and lithium bis (trifuluoro-methylsulfonyl) imide (0.031 M), tris [2-(1H-pyrazol-1-y1)-4-tert-butylpyridine] cobalt (III) tris [bis(trifluoromethysulfonyl) imide] (5.6×10^{-3} M) as dopants.[28, 29] The films were left on a hot plate for annealing in the glove box at 70 °C for 20 min. The films were then placed in a vacuum chamber and 100 nm thick silver electrodes were deposited on the spiro-OMeTAD layer with a pressure at around 2.83×10^{-4} pa. The active device area was 4 mm^2. The current densities versus voltage (J-V) characteristics of the cells were analyzed under simulated AM 1.5G solar illumination with Keithley 2401 Digital Source Meter.

Results and Discussion

The chemical structure of HMImCl is shown in Fig. 1a. We introduced 1 wt% of HMImCl to the solution of $MAPbI_3$ in DMF as a morphology-controlling additive. The IL-doped solution of $MAPbI_3$ was a homogeneous clear yellow-orange, because no aggregate or NPs were observed in it (Fig. 1b). The process

RSC Advances Accepted Manuscript

This journal is © The Royal Society of Chemistry 20xx

used to fabricate $MAPbI_3$ films with/without IL via spin coating is schematically illustrated in Fig. 1c.

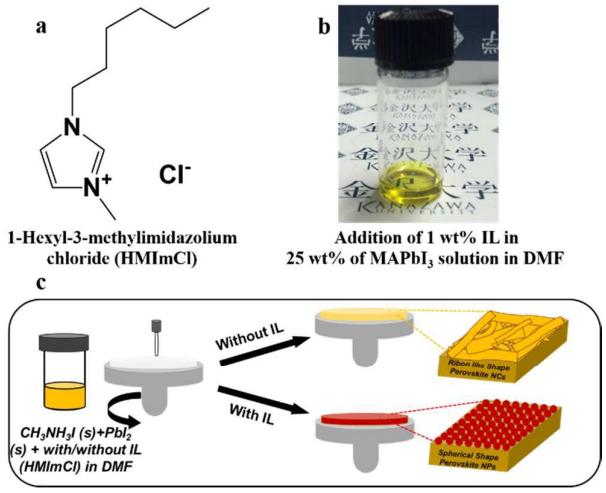

Fig. 1. (a) Chemical structure of HMImCl. (b) Photograph of a homogeneous solution of $MAPbI_3$ in DMF containing 1 wt% IL. (c) Schematic of perovskite film formation with/without IL.

Figure 2a–b reveal that the films processed without IL have incomplete surface coverage and are composed of non-uniform large crystals with a ribbon-like shape. These observations are similar to those in a previous report by Xiao et al.,[30] which confirms that the non-uniformity in the perovskite film was caused by the rapid evaporation of DMF during spin coating. In contrast, uniform $MAPbI_3$ NPs with a well-controlled spherical shape and an average diameter of 540 nm were observed when 1 wt% IL was added to the spin-coating solution (Fig. 2c–d). This observation is further confirmed by the AFM analysis (Fig. 3a, b). The RMS roughness for the perovskite films with and without IL were, 23.4 and 76.1 nm, respectively. These data support the formation of a smooth uniform NP film by inclusion of an IL in the spin-coating solution. A uniform air-stable amorphous TiO_x layer with a thickness of 30 nm was prepared, as shown in AFM analysis (Fig. 3c). The RMS roughness of the amorphous film was 3.13 nm. The morphologies of the films produced at room temperature (RT) as determined by AFM (Fig. 3d). Figure 3d reveals that the small clusters formed at RT remained aggregated and was not uniformly distributed. The RMS roughness of the film was 46.5 nm as deposited film.

The EDX-mapping (Fig. 4a-f) was performed to address the question of whether the $MAPbI_3$ films, processed with and without IL, are composed of single or multiple phases. The technique allowed us to visualize a two-dimensional map of the relative location of the different elements in the sample. The color intensity assists to judge the relative amount of element distributed in the surface. The EDX-analysis of $MAPbI_3$ films showed mostly similar in both cases (with/without IL) the ratio Pb to I is around 21/64 in good agreement with a PbI_3 stoichiometry.

The XRD patterns of the perovskite films formed with and without IL, recorded at 100 °C, are shown in Fig. 5. It has been

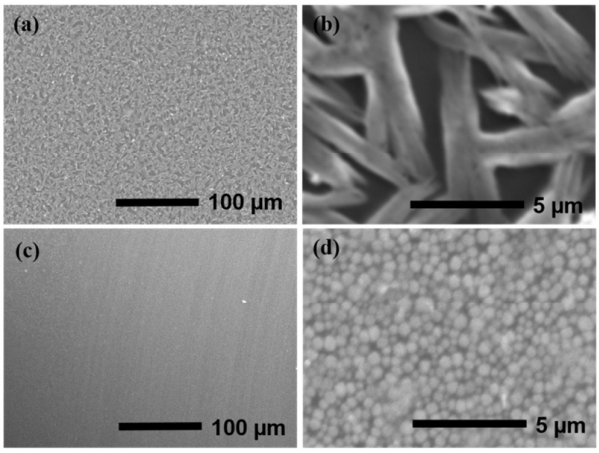

Fig. 2 The low- and high-magnification SEM images of $MAPbI_3$ films prepared without IL (a, b) and with IL (c, d), respectively.

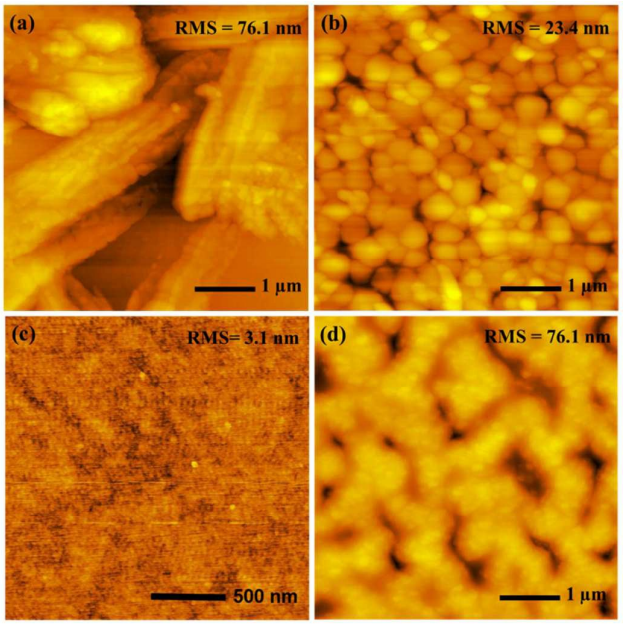

Fig. 3 AFM images of $MAPbI_3$ films prepared by spin coating (a) without and (b) with the addition of IL to control morphology; (c) air-stable uniform compact TiO_x film prepared by CBD; (d) $MAPbI_3$ small clusters prepared at RT.

reported that the complete formation of perovskite film with full surface coverage is achieved at 100 °C [31] and, hence, selected for subsequent experiments. At temperatures lower than 100 °C, the NP films remained aggregated and were not uniformly distributed. Moreover, if the temperature is ≥ 120 °C, the decomposition of $MAPbI_3$ is initiated and induces poor film coverage.[32] The diffraction peaks of the perovskite films prepared at 100 °C were observed at 2θ = 14.01°, 28.40°, 31.91°, and 40.74° for films both with and without IL, and are assigned to the (110), (220), (310) and (224) crystal planes, respectively. These peak positions are consistent with an

RSC Advances Accepted Manuscript

orthorhombic crystalline structure in both films.[24, 33] It should be noted that there was no PbI_2 peak at 12.65° in either of the XRD patterns, which indicates the complete consumption of PbI_2. The mean crystallite sizes for the perovskite crystals formed with and without IL were 35.8 and 37.5 nm, respectively, estimated from the full width at half-maximum of the (110) peak using the Scherrer formula. (See supporting information; Table S1). These results indicate that the crystallinity is almost similar, even after the addition of IL.

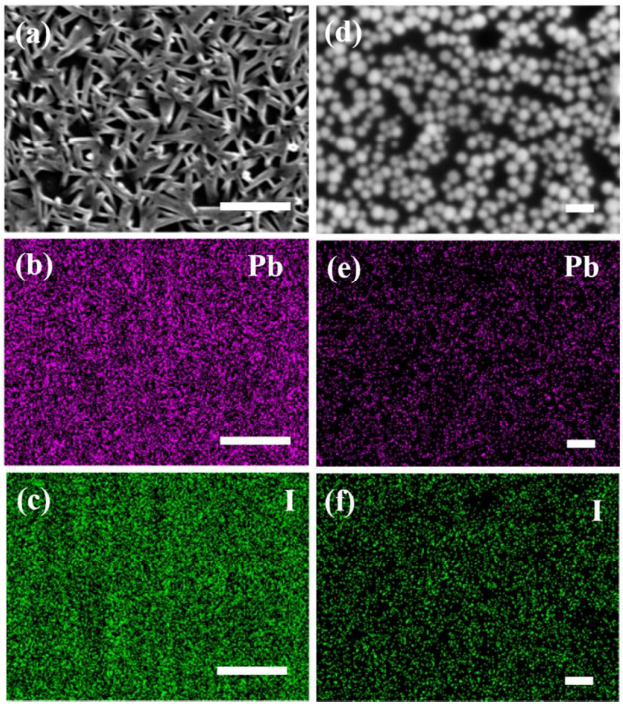

Fig. 4 (a) The dark field images of $MAPbI_3$ film formed without IL and EDX mapping of (b) lead and (c) iodine (10 µm scale bar for all); (d) the dark field images of $MAPbI_3$ film formed with IL and EDX maps of (e) lead and (f) iodine (2.5 µm scale bar for all).

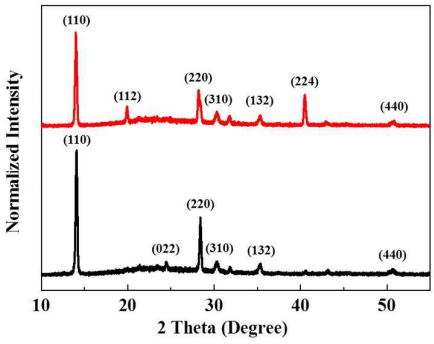

Fig. 5. The XRD patterns of $MAPbI_3$ films formed with (red color) and without IL (black color).

The existence of the IL additive within the $MAPbI_3$ films was confirmed from the FTIR spectra (Fig. 6). The FTIR reveals that the IL molecules are adsorbed on the surface of the $MAPbI_3$ NPs as indicated by the absorption bands in the region of 2,650 to 3,000 cm^{-1}, which are assigned to C–H stretching of the imidazolium ring. The observation was similar to a pervious report by Ayi et al [34], which confirms that the molecules of IL are absorbed on the surface of the particles thus provides protection during the formation of nanostructured particles. The bands at 3,200–3,300 cm^{-1} along with the bands between 1,500 and 1,700 cm^{-1} can be attributed to N-H stretching and bending vibrational bands. The N-H bending vibration reveals that IL molecules intercalated into $MAPbI_3$ NPs films. The findings of both the C-H and N-H deformation modes in the $MAPbI_3$ NPs film assure the successful inclusion of IL.

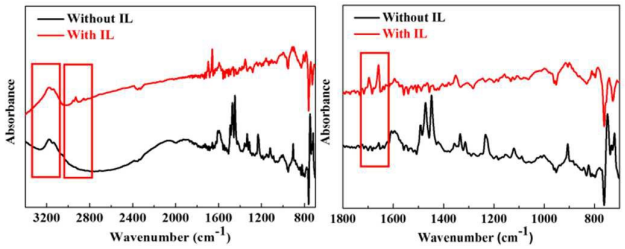

Fig. 6. The FTIR spectra of $MAPbI_3$ films with and without IL.

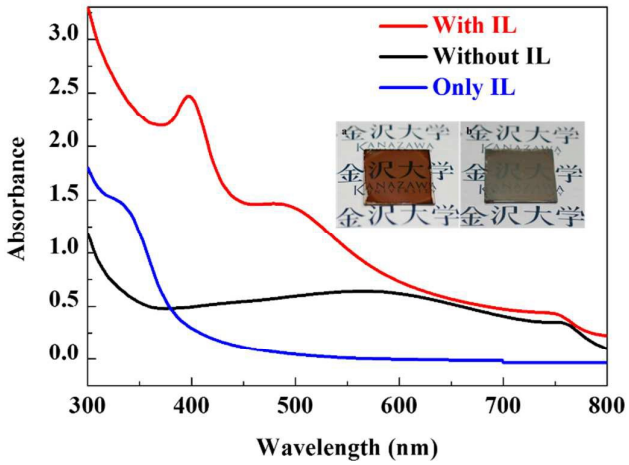

Fig. 7. The UV-Vis spectra of only IL and $MAPbI_3$ films prepared with and without IL. Inset photographs show $MAPbI_3$ films prepared with (left) and without (right) IL.

The UV-Vis spectra of $MAPbI_3$ films, with and without IL, on glass/ITO/TiO_x substrates are shown in Fig. 7. The maximum absorption spectrum for DMF is observed at around 263 nm (not shown in Figure), while it is at around 340 nm for only IL. The strong absorption peaks as observed at around 493 and 396 nm in the system with IL correspond to the imidazolium cation and NPs, respectively.[34] The observation of UV-Vis study is further verified using the SEM technique. The film produced without IL absorbed more strongly at > 500 nm than that formed with IL, which can be attributed to the formation of pin holes and incomplete coverage of the $MAPbI_3$ film. In contrast, the film produced with IL showed a curve at < 500 nm, which indicated higher optical density than that of the film formed

RSC Advances Accepted Manuscript

This journal is © The Royal Society of Chemistry 20xx

without IL. The inset of Fig. 7 shows photographs of patterned glass/ITO/TiO_x substrates with $MAPbI_3$ films formed with and without IL. The thin film of $MAPbI_3$ NPs produced with IL was red-brown in color, flat in shape, and the surface coverage was uniform and free of pin-holes. Conversely, the $MAPbI_3$ nanocrystals formed without IL had a non-uniform surface, were scattered, and the film color was shiny gray.

The $MAPbI_3$ nanocrystals formed without IL were ribbon like because of their rapid formation during spin coating caused by the fast evaporation of DMF. Such conditions promoted fast nucleation; therefore, the produced film remained incomplete and non-homogeneous. Jeon *et al.*[35] reported a similar occurrence with $MAPbI_3$ NC formation.

The formation mechanism for the $MAPbI_3$ NPs is illustrated in Fig. 8. The $MAPbI_3$/DMF/IL solution was spun cast under the optimized conditions. During the spin-coating process, small clusters were formed, followed by homogeneous nucleation to generate NPs. These steps are consistent with the AFM analysis of the deposited film (Fig. 3d). Because of intercalation, the IL remained in the film, while the residual fraction of DMF evaporated. Small clusters were bonded to the nucleation sites, which then grew to form uniform spherical $MAPbI_3$ NP films. The $MAPbI_3$ NPs were forced to align perpendicular to the c-axis because of the high boiling point and extremely low vapor pressure of the IL. The surface energy of the prismatic plane was higher than that of the basal plane. In the presence of IL, whenever a crystal grew, it tried to minimize the overall surface energy, which promoted crystal growth in the *c*-axis direction.

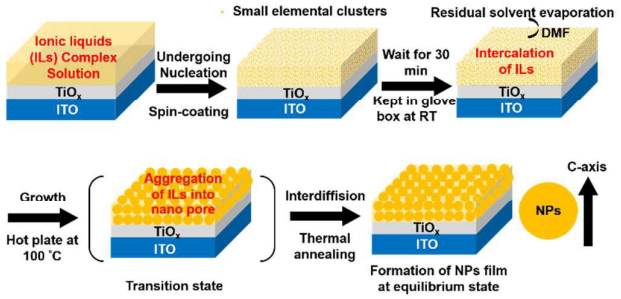

Fig. 8. Schematic of the formation mechanism of $MAPbI_3$ NPs.

The current density versus voltage (J-V) characteristics of $MAPbI_3$ films with/without IL measured at AM 1.5G illumination is shown in Fig. 9b. The device without IL showed a short-circuit current density J_{sc} of 11.90 mA/cm^2, V_{oc} = 0.92 V, FF = 0.49, and PCE = 5.10 %. On the contrary, the device with IL displayed J_{sc} = 4.84 mA/cm^2, V_{oc} = 0.78 V, FF = 0.64, and PCE = 2.44 %. The PCE was lower than the reference material (without IL) presumably due to the presence of ionic liquids (IL) in the films.

The preliminary results are promising as it is the first report on the fabrication of solar cells based on $MAPbI_3$ NPs. We also expect that the results will open a pathway towards a better understanding for the fabrication, modification and

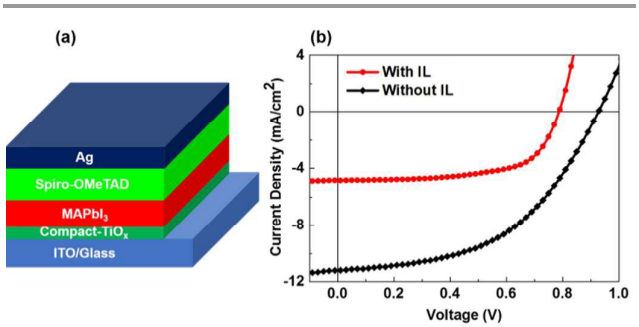

Fig. 9. (a) Device structure of solar cells based on $MAPbI_3$; (b) The J-V characteristics obtained for the solar cells based on $MAPbI_3$ with and without IL.

enhancement of the performance of solar cells with $MAPbI_3$ NPs. In the present case, we assume a hindering effect followed by impact on charge dissociation, transport, and/or recombination on the device performances due to the residual IL content remained on the $MAPbI_3$ NP films. Therefore, we have assumed that a non-destructive solvent-assisted washing procedure is required to be included to remove the IL from $MAPbI_3$ NP film, which is shown schematically in Fig. 10. The idea was inspired from the observation for small molecule-$MAPbI_3$ medium by Chen et al.[36] It is also reported that the adverse effect of small molecules trapped inside the perovskite sensitizer causing charge recombination can be minimized after solvent washing.[37] We hope that we will be able to ensure the complete removal of IL-contents from the $MAPbI_3$ NP film after establishing an optimized condition using a suitable solvent, and the efficiency of the resulting solar cell will be improved.

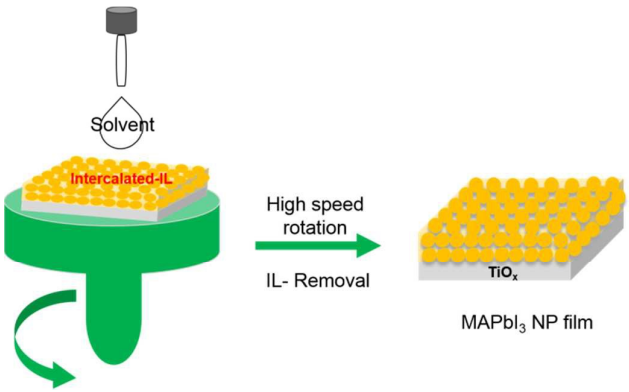

Fig. 10. Schematic illustration of solvent additive procedure for preparing $MAPbI_3$ NP film.

Conclusions

We fabricated spherical NPs of $MAPbI_3$ using a simple spin-coating method by incorporating a small amount (1 wt%) of an IL in the spin-coating solution. The $MAPbI_3$ NP thin films were uniform and free of pin holes, and the excellent morphology was due to the addition of IL. The light-absorption property has also been improved. The photovoltaic properties of

RSC Advances Accepted Manuscript

perovskite solar cells have been studied, and the preliminary performance data indicate that the $MAPbI_3$ NPs could be used to design unique solar cells.

Acknowledgements

We thank Dr. Takuya Tsujiguchi of Kanazawa University for SEM measurements.

References

1. T. He, Q. Huang, A. P. Ramirez, Y. Wang, K. A. Regan, N. Rogado, M. A. Hayward, M. K. Haas, J. S. Slusky, K. Inumara, H. W. Zandbergen, N. P. Ong and R. J. Cava, *Nature*, 2001, **411**, 54–56.
2. S. Yasuhiro, F. Yoshiki, A. Hiromichi and S. Tetsuro, in *Fundamentals and Applications of Chemical Sensors*, American Chemical Society, 1986, vol. 309, pp. 83–100.
3. S. Tao and J. T. S. Irvine, *Nat. Mater.*, 2003, **2**, 320–323.
4. M. E. Lines and A. M. Glass, *Principles and Applications of Ferroelectrics and Related Materials (Monographs on Physics)*, Clarendon Press, Oxford, England, 1977.
5. P. M. Rørvik, T. Grande and M.-A. Einarsrud, *Adv. Mater.*, 2011, **23**, 4007–4034.
6. H. Kato and A. Kudo, *J. Phys. Chem. B*, 2001, **105**, 4285–4292.
7. J. Suntivich, H. A. Gasteiger, N. Yabuuchi, H. Nakanishi, J. B. Goodenough and Y. Shao-Horn, *Nat. Chem.*, 2011, **3**, 546–550.
8. Y. Zhao, L. Xu, L. Mai, C. Han, Q. An, X. Xu, X. Liu and Q. Zhang, *P. Natl. Acad. Sci. USA*, 2012, **109**, 19569–19574.
9. L. Bocher, M. H. Aguirre, D. Logvinovich, A. Shkabko, R. Robert, M. Trottmann and A. Weidenkaff, *Inorg. Chem.*, 2008, **47**, 8077–8085.
10. M. C. Beard, J. M. Luther and A. J. Nozik, *Nat. Nanotechnol.*, 2014, **9**, 951–954.
11. Y. Mao, T.-J. Park and S. S. Wong, *Chem. Commun.*, 2005, 5721–5735.
12. T. Ishihara, J. Takahashi and T. Goto, *Phys. Rev.*, 1990, **42**.
13. J. Calabrese, N. L. Jones, R. L. Harlow, N. Herron, D. L. Thorn and Y. Wang, *J. Am. Chem. Soc.*, 1991, **113**, 2328–2330.
14. S. Wang, D. B. Mitzi, C. A. Feild and A. Guloy, *J. Am. Chem. Soc.*, 1995, **117**, 5297–5302.
15. Y. Takeoka, K. Asai, M. Rikukawa and K. Sanui, *Chem. Lett.*, 2005, **34**, 602–603.
16. T. Yang, Z. D. Gordon and C. K. Chan, *Cryst. Growth Des.*, 2013, **13**, 3901–3907.
17. Z. Deng, Y. Dai, W. Chen, X. Pei and J. Liao, *Nanoscale Res. Lett.*, 2010, **5**, 1217–1221.
18. W. Dong, B. Li, Y. Li, X. Wang, L. An, C. Li, B. Chen, G. Wang and Z. Shi, *J. Phys. Chem. C*, 2011, **115**, 3918–3925.
19. N. C. Pramanik, S. I. Seok and B. Y. Ahn, *J. Colloid Interf. Sci.*, 2006, **300**, 569–576.
20. A. P. Bartlett, M. Pichumani, M. Giuliani, W. González−Viñas and A. Yethiraj, *Langmuir*, 2012, **28**, 3067–3070.
21. L. C. Schmidt, A. Pertegás, S. González-Carrero, O. Malinkiewicz, S. Agouram, G. Mínguez Espallargas, H. J. Bolink, R. E. Galian and J. Pérez-Prieto, *J. Am. Chem. Soc.*, 2014, **136**, 850-853.
22. E. Horváth, M. Spina, Z. Szekrényes, K. Kamarás, R. Gaal, D. Gachet and L. Forró, *Nano Lett.*, 2014, **14**, 6761–6766.
23. J. Y. Jeng, Y. F. Chiang, M. H. Lee, S. R. Peng, T. F. Guo, P. Chen and T. C. Wen, *Adv Mater*, 2013, **25**, 3727-3732.
24. P.-W. Liang, C.-Y. Liao, C.-C. Chueh, F. Zuo, S. T. Williams, X.-K. Xin, J. Lin and A. K. Y. Jen, *Adv. Mater.*, 2014, **26**, 3748–3754.
25. P. Docampo, J. M. Ball, M. Darwich, G. E. Eperon and H. J. Snaith, *Nat Commun*, 2013, **4**, 2761.
26. T. Kuwabara, H. Sugiyama, M. Kuzuba, T. Yamaguchi and K. Takahashi, *Org. Electron.*, 2010, **11**, 1136–1140.
27. K. Yamamoto, Y. Zhou, K. T, K. Takahashi and T. Taima, in *Photovoltaic Specialist Conference (PVSC), 2014 IEEE 40th*, IEEE, Denver, CO, 2014, pp. 1573–1576.
28. A. Wakamiya, M. Endo, T. Sasamori, N. Tokitoh, Y. Ogomi, S. Hayase and Y. Murata, *Chem. Lett.*, 2014, **43**, 711-713.
29. A. Dualeh, T. Moehl, N. Tétreault, J. Teuscher, P. Gao, M. K. Nazeeruddin and M. Grätzel, *ACS Nano*, 2014, **8**, 362-373.
30. M. Xiao, F. Huang, W. Huang, Y. Dkhissi, Y. Zhu, J. Etheridge, A. Gray-Weale, U. Bach, Y.-B. Cheng and L. Spiccia, *Angew. Chem.*, 2014, **53**, 9898–9903.
31. A. Dualeh, N. Tétreault, T. Moehl, P. Gao, M. K. Nazeeruddin and M. Grätzel, *Adv. Funct. Mater.*, 2014, **24**, 3250-3258.
32. G. E. Eperon, V. M. Burlakov, P. Docampo, A. Goriely and H. J. Snaith, *Adv. Funct. Mater.*, 2014, **24**, 151-157.
33. Q. Chen, H. Zhou, Z. Hong, S. Luo, H.-S. Duan, H.-H. Wang, Y. Liu, G. Li and Y. Yang, *J. Am. Chem. Soc.*, 2013, **136**, 622–625.
34. A. A. Ayi, C. A. Anyama and S. S. Etuk, *J. Appl. Chem.*, 2014, **2**, 26–32.
35. Y.-J. Jeon, S. Lee, R. Kang, J.-E. Kim, J.-S. Yeo, S.-H. Lee, S.-S. Kim, J.-M. Yun and D.-Y. Kim, *Sci. Rep.*, 2014, **4**, 6953.
36. C.-C. Chen, Z. Hong, G. Li, Q. Chen, H. Zhou and Y. Yang, *Journal of Photonics for Energy*, 2015, **5**, 057405-057405.
37. N. J. Jeon, J. H. Noh, Y. C. Kim, W. S. Yang, S. Ryu and S. I. Seok, *Nat. Mater.*, 2014, **13**, 897-903.

RSC Advances Accepted Manuscript

This journal is © The Royal Society of Chemistry 20xx